Eur. Phys. J. C (2026) 86:553
https://doi.org/10.1140/epjc/s10052-026-15812-y

THE EUROPEAN PHYSICAL JOURNAL C

Regular Article - Theoretical Physics

Anisotropic shear-free radiating collapse: exact solutions and numerical validation

Kali Charan[1,a], **Om Prakash Yadav**[2,b], **B. C. Tewari**[3,4,c]

[1] Institute of Applied Sciences, Mangalayatan University, Aligarh 202146, India
[2] Department of Mathematics and Scientific Computing, National Institute of Technology Hamirpur, Hamirpur, Himachal Pradesh, India
[3] Department of Mathematics, Kumaun University, SSJ Campus Almora, Almora, India
[4] Kshitij, Tuni Khirkhet, Ranikhet, Distt, Almora 263645, Uttarakhand, India

Received: 7 March 2026 / Accepted: 7 May 2026

Abstract We construct a new class of exact solutions for shear-free, spherically symmetric radiating stars undergoing gravitational collapse in the presence of pressure anisotropy. Starting with the static metric potentials, we specialise the parametric family to the inhomogeneous anisotropic subclass $n = -2$ and carry out a complete dynamical and thermodynamic analysis of this configuration. The interior solution, obtained in closed form, satisfies the standard regularity and energy conditions (null, weak, strong, and dominant), and is matched across the stellar boundary to an exterior Vaidya spacetime through the appropriate junction conditions. The configuration admits an initially static perfect-fluid limit and evolves smoothly into a dissipative collapse driven by radiative heat transport. A numerical study is also performed, wherein the effect of the anisotropy parameter on radial profiles and temporal evolutions of the density, pressures, heat flux, collapse rate, redshift, luminosity, and interior temperature is studied. The energy conditions are verified. The results demonstrate that increasing pressure anisotropy strengthens the matter variables, accelerates the contraction rate and enhances thermal dissipation throughout the radiating phase.

1 Introduction

Radiative collapse and black hole formation remain active areas of research in general relativity, with new insights continuing to emerge on observational and theoretical fronts. Recently mergers of exceptionally massive black holes (in the "forbidden" mass-gap range) have lent further impetus to ongoing efforts to develop a deeper and more comprehensive understanding of their formation and evolution [1]. Modern developments trace their theoretical roots to the pioneering field equations of Einstein [2] and the first exact exterior solution of Schwarzschild [3], which laid the foundations of gravitational physics. The existence of limiting masses for compact remnants and the inevitability of collapse for sufficiently massive configurations were clarified by Chandrasekhar [4] and by Oppenheimer and Snyder [5]. While the Oppenheimer–Snyder dust model is idealised, it established the basic picture that collapse can proceed toward horizon formation under appropriate conditions.

Realistic collapse process is intrinsically heat dissipative. In late evolutionary stages, neutrino emission, photon diffusion, and heat transport remove energy from the interior and modify the rate of contraction. Outgoing radiation is described by the Vaidya exterior spacetime [6], whose physical interpretation was discussed by Lindquist et al. [7]. For radiating stars, matching a collapsing interior to a Vaidya exterior requires junction conditions on the boundary surface; the key relations connecting surface pressure and heat flow were established by Santos [8], enabling systematic investigations of shear-free radiating interiors [9].

Within this framework, de Oliveira et al. studied radiating collapse and horizon formation using diffusion-based descriptions [10], and exact interior solutions matched to the Vaidya exterior were later presented by de Oliveira and Santos [11]. A comprehensive review of radiating spherical collapse was given by Bonnor et al. [12]. Subsequent work emphasised the role of Weyl stresses [13], generating functions for shear-free collapse [14], and the influence of different thermodynamic and transport assumptions [15,16]. Scenarios in which the collapse remains radiative while delaying or avoiding horizon formation have also been explored [17].

[a] e-mail: kali.charan@mangalayatan.edu.in
[b] e-mail: opyadav@nith.ac.in (corresponding author)
[c] e-mail: drbctewari@yahoo.co.in

Published online: 20 May 2026

The influence of shear on dissipative collapse was investigated by Chan [18], who demonstrated its significant impact on the thermal and dynamical evolution. This analysis was extended to the charged case by Maharaj and Govender [19]. Further developments in exact modelling of radiating stars include generalized Euclidean stellar configurations with a barotropic equation of state [20] and the study of two-fluid atmospheric effects on relativistic stellar structure [21]. Maharaj and Brassel constructed radiating models with composite matter distributions, both in the neutral [22] and electromagnetically charged [23] settings.

Pressure anisotropy is an important naturally and physically motivated component that can substantially alter collapse dynamics. Anisotropic stresses may arise, among others, from superfluid components, phase transitions, strong magnetic fields, viscosity. Their role in relativistic spheres has been discussed since the early work of Bowers and Liang [24]. Static anisotropic stellar models have been investigated across a variety of geometries and gravitational theories, including higher-dimensional spacetimes [25], generalised compact star frameworks [26], and ultracompact configurations in general relativity where pressure anisotropy supports objects more compact than their isotropic counterparts [27]. Specific geometric ansätze have been employed to construct anisotropic models in Vaidya–Tikekar spacetime with the MIT bag model equation of state [28], Finch–Skea geometry in Einstein–Gauss–Bonnet gravity [29], and charged stars [30,31]. A general account of local anisotropy in self-gravitating systems was provided by Herrera and Santos [32]. Further exact anisotropic constructions in various settings are explored in [33–35], while the effect of anisotropy on stellar structure and compact-star models has been investigated through gravitational decoupling and other approaches [36–38]. In dissipative collapse, anisotropy modifies the effective inertial mass density and the balance between gradients, heat flow, thereby shifting horizon formation times and thermal evolution. This interplay has been examined in dissipative models with anisotropic stresses in [39,40], including analyses of the resulting temperature behaviour in [41]. More recent work continues to refine analytic and numerical solutions of radiating models using various techniques [42–49].

Motivated by these results, we construct and analyse a shear-free, spherically symmetric radiating collapse model in which pressure anisotropy serves as the primary control parameter. The interior satisfies standard regularity, energy, and thermodynamic conditions and is matched smoothly to the Vaidya exterior at the boundary. Starting from an initially static configuration, the system evolves into a radiating collapse governed by the junction conditions. We obtain exact relations for all interior variables and present numerical study for representative parameter sets. The plots and numerical discussions isolate how increasing anisotropy changes the density and pressures, accelerates the collapse rate, modifies the redshift and luminosity at infinity.

In this work, we derive exact solutions by proposing the ansatz $f(t) = g(t)$ and obtain the associated physical quantities. A complete dynamical analysis of the inhomogeneous anisotropic subclass ($n = -2$) is carried out, yielding closed-form expressions for the density, pressures, heat flux, collapse rate, mass function, luminosities, redshift, and black hole formation time. Furthermore, a systematic numerical study is performed in which the anisotropy parameter $\delta(r)$ is varied through C_1 across three representative levels (low, moderate, high), thereby isolating the quantitative role of pressure anisotropy on all interior and surface observables. The null, weak, strong, and dominant energy conditions are also verified for the chosen parameter ranges.

The rest of the article is organized as follows. Section 2 outlines the formulation of the problem, including the field equations and junction conditions. Section 3 presents the solution of the field equations by introducing a separability ansatz for the metric potentials and deriving the expression for the collapse function. Section 4 develops the parametric class of exact anisotropic solutions, while Sect. 5 derives the general structure of the matter variables for the collapsing radiating star. Section 6 specialises these solutions to the case $n = -2$, yielding explicit forms for the density, pressures, heat flux, and collapse rate and Sect. 7 is devoted to the verification of energy conditions and study of temperature evolution. Finally, Sect. 8 contains our conclusions.

Notations and symbols

Some symbols used throughout this paper are listed below for convenience (Table 1).

Table 1 List of principal symbols

Symbol	Description
Derivatives and symbols	
$()' \equiv \partial/\partial r$	Prime denotes partial derivative with respect to r
$\dot{()} \equiv \partial/\partial t$	Overdot denotes partial derivative with respect to t
$()_{,\nu}$	Partial derivative with respect to coordinate x^ν
$()_{;\nu}$	Covariant derivative with respect to coordinate x^ν
$()_\Sigma$	Quantity evaluated at the boundary $r = r_\Sigma$
$()_0$	Quantity evaluated for the static configuration
Other variables	
$M^-,\ M^+$	Interior and exterior spacetime regions
Σ	Stellar boundary hypersurface
v	Retarded time (Vaidya exterior)
r_Σ	Radial coordinate of the boundary surface
$\epsilon,\ p_r,\ p_t$	Energy density, radial and tangential pressures
$\delta(r)$	Anisotropy function (radial part)

2 Field equations and junction conditions

The space-time environment of a radiating star is naturally partitioned by the stellar boundary into two distinct regions: the interior space-time M^- and the exterior space-time M^+. Every region is characterised by a smooth, time-like three-dimensional hypersurface whose boundary is represented by Σ. The matching across Σ is performed by requiring continuity of both the first and second fundamental forms. Thus,

$$(ds_+^2)_\Sigma = (ds_-^2)_\Sigma = ds_\Sigma^2, \tag{2.1}$$

and

$$K_{ij}^- = K_{ij}^+, \tag{2.2}$$

where

$$K_{ij}^\pm = -n_\mu^\pm \left(\frac{\partial^2 \chi_\pm^\mu}{\partial \xi^i \partial \xi^j} + \Gamma^\mu_{\nu\eta} \frac{\partial \chi_\pm^\nu}{\partial \xi^i} \frac{\partial \chi_\pm^\eta}{\partial \xi^j} \right).$$

Here, $\chi_\pm^\mu$ denote the coordinates in $M^\pm$, ξ^i are the intrinsic coordinates on Σ, and $n_\mu^\pm$ are the unit normal vectors to Σ.

We consider a spherically symmetric, collapsing fluid that dissipates energy through heat flow, bounded by a time-like spherical surface Σ having the induced metric,

$$ds_\Sigma^2 = -d\tau^2 + \mathcal{R}^2(\tau) \left(d\theta^2 + \sin^2\theta \, d\phi^2 \right). \tag{2.3}$$

For a shear-free, spherically symmetric fluid interior, the metric is given by,

$$ds_-^2 = -A^2(r,t)\, dt^2 + B^2(r,t) \left\{ dr^2 + r^2 \left(d\theta^2 + \sin^2\theta \, d\phi^2 \right) \right\}. \tag{2.4}$$

The energy–momentum tensor modeling the matter content, that accounts for pressure anisotropy, is given by,

$$T_{\mu\nu} = (\epsilon + p_t)\, w_\mu w_\nu + p_t\, g_{\mu\nu} + (p_r - p_t)\, x_\mu x_\nu + q_\mu w_\nu + q_\nu w_\mu, \tag{2.5}$$

where ϵ is the fluid energy density, p_r and p_t are the radial and tangential pressures, w_μ is the four-velocity, q_μ is the radial heat flux vector, and x_μ is a unit space-like four-vector along the radial direction.

In comoving coordinates, the four-velocity becomes,

$$w^\mu = \frac{1}{A}\, \delta_0^\mu. \tag{2.6}$$

The heat flux vector q^μ is orthogonal to w^μ, that is $q^\mu w_\mu = 0$, and therefore,

$$q^\mu = q\, \delta_1^\mu. \tag{2.7}$$

The metric (2.4) describes a shear-free configuration, as the shear tensor vanishes identically. The fluid expansion scalar $\Theta = w^\mu{}_{;\mu}$ is given by,

$$\Theta = \frac{3\dot{B}}{AB}. \tag{2.8}$$

The non-trivial Einstein field equations, arising from (2.4) and (2.5), form the following system,

$$\kappa\epsilon = -\frac{1}{B^2}\left(\frac{2B''}{B} - \frac{B'^2}{B^2} + \frac{4B'}{rB} \right) + \frac{3\dot{B}^2}{A^2B^2}, \tag{2.9}$$

$$\kappa p_r = \frac{1}{B^2}\left(\frac{B'^2}{B^2} + \frac{2A'B'}{AB} + \frac{2A'}{rA} + \frac{2B'}{rB} \right) + \frac{1}{A^2}\left(-\frac{2\ddot{B}}{B} - \frac{\dot{B}^2}{B^2} + \frac{2\dot{A}\dot{B}}{AB} \right), \tag{2.10}$$

$$\kappa p_t = \frac{1}{B^2}\left(\frac{B''}{B} - \frac{B'^2}{B^2} + \frac{B'}{rB} + \frac{A''}{A} + \frac{A'}{rA} \right) + \frac{1}{A^2}\left(-\frac{2\ddot{B}}{B} - \frac{\dot{B}^2}{B^2} + \frac{2\dot{A}\dot{B}}{AB} \right), \tag{2.11}$$

$$\kappa q = -\frac{2}{AB^2}\left(-\frac{\dot{B}'}{B} + \frac{B'\dot{B}}{B^2} + \frac{A'\dot{B}}{AB} \right), \tag{2.12}$$

where primes and overdots denote partial differentiation with respect to r and t, respectively. Throughout, we work in geometrised units with $\kappa = 8\pi$ (i.e. $G = c = 1$).

The exterior space-time is described by the Vaidya metric, which models an outgoing radial flux of radiation,

$$ds_+^2 = -\left(1 - \frac{2M(v)}{R}\right) dv^2 - 2\, dR\, dv + R^2 \left(d\theta^2 + \sin^2\theta \, d\phi^2 \right), \tag{2.13}$$

where v is the retarded time coordinate and $M(v)$ is the exterior Vaidya mass.

The matching of the interior space-time (2.4) with the exterior Vaidya space-time (2.13) across the boundary hypersurface Σ is performed by requiring continuity of both the first and second fundamental forms, given in (2.1) and (2.2). Thus, the resulting junction conditions are

$$(rB)_\Sigma = R_\Sigma(v) = \mathcal{R}(\tau), \tag{2.14}$$

$$(p_r)_\Sigma = (qB)_\Sigma, \tag{2.15}$$

$$m_\Sigma(r,t) = M(v) = \left\{ \frac{r^3 B \dot{B}^2}{2A^2} - r^2 B' - \frac{r^3 B'^2}{2B} \right\}_\Sigma, \tag{2.16}$$

where m_Σ is the Misner–Sharp mass evaluated at the boundary $r = r_\Sigma$. Equation (2.14) follows from continuity of the first fundamental form, whereas Eqs. (2.15) and (2.16) arise from continuity of the second fundamental form.

The surface luminosity measured at Σ is,

$$L_\Sigma = \frac{\kappa}{2} \left\{ r^2 B^3 q \right\}_\Sigma, \tag{2.17}$$

and the boundary redshift is,

$$z_\Sigma = \left\{ \frac{r(Br)' - r^2\left(\frac{B}{A}\right)\dot{B}}{rB - 2M} \right\}_\Sigma - 1. \tag{2.18}$$

The total luminosity as measured by a distant static observer is related to the rate of mass loss,

$$L_\infty = -\frac{dM}{dv} = \frac{L_\Sigma}{(1+z_\Sigma)^2}. \tag{2.19}$$

3 Solution of the field equations

To solve the field equations, we assume a specific form of the metric coefficients in Eq. (2.4) by expressing them explicitly as functions of the radial coordinate r and time t. This choice simplifies the system of equations by separating the radial and temporal dependencies, thereby facilitating the integration process and enabling the determination of the associated physical quantities

$$A(r,t) = A_0(r)\, g(t) \tag{3.1}$$

$$B(r,t) = B_0(r)\, f(t) \tag{3.2}$$

In view of Eqs. (3.1) and (3.2), substitution of the corresponding metric functions and auxiliary relations into Einstein's field equations (2.9)–(2.12) yields a reduced and explicit system of coupled differential equations. Thus, by incorporating the forms given in (3.1) and (3.2), the original field equations transform into a consistent system that describes the dynamical evolution of the configuration

$$\kappa\epsilon = \frac{\epsilon_0}{f^2} + \frac{3\dot{f}^2}{A_0^2 g^2 f^2}, \tag{3.3}$$

$$\kappa p_r = \frac{(p_r)_0}{f^2} + \frac{1}{A_0^2 g^2}\left(-\frac{2\ddot{f}}{f} - \frac{\dot{f}^2}{f^2}\right), \tag{3.4}$$

$$\kappa p_t = \frac{(p_t)_0}{f^2} + \frac{1}{A_0^2 g^2}\left(-\frac{2\ddot{f}}{f} - \frac{\dot{f}^2}{f^2}\right), \tag{3.5}$$

$$\kappa q = -\frac{2A_0'\dot{f}}{A_0^2 B_0^2\, g\, f^3}, \tag{3.6}$$

where

$$\epsilon_0 = -\frac{1}{B_0^2}\left(\frac{2B_0''}{B_0} - \frac{B_0'^2}{B_0^2} + \frac{4B_0'}{rB_0}\right), \tag{3.7}$$

$$(p_r)_0 = \frac{1}{B_0^2}\left(\frac{B_0'^2}{B_0^2} + \frac{2B_0'}{rB_0} + \frac{2A_0'B_0'}{A_0B_0} + \frac{2A_0'}{rA_0}\right), \tag{3.8}$$

$$(p_t)_0 = \frac{1}{B_0^2}\left(\frac{B_0''}{B_0} - \frac{B_0'^2}{B_0^2} + \frac{B_0'}{rB_0} + \frac{A_0''}{A_0} + \frac{A_0'}{rA_0}\right). \tag{3.9}$$

Here, the quantities carrying the subscript 0 refer to the corresponding variables of the static stellar configuration. In this context, they are evaluated with respect to the static metric potentials $A_0(r)$ and $B_0(r)$, which describe the equilibrium geometry of the star prior to the onset of dynamical evolution.

In the absence of dissipative effects, the boundary condition given by Eq. (2.15), $(p_r)_\Sigma = (qB)_\Sigma$ simplifies accordingly. Since the heat flux vanishes in the non-dissipative case, this relation reduces to the requirement that the radial pressure at the boundary must be zero. Consequently, one obtains the condition $\{(p_r)_0\}_\Sigma = 0$, which is satisfied at the stellar surface $r = r_\Sigma = R_\Sigma$. This expresses the standard matching condition for a static configuration, where the interior solution joins smoothly to the exterior spacetime at the boundary

$$\frac{2\ddot{f}}{f} + \frac{\dot{f}^2}{f^2} - \frac{2\dot{g}\dot{f}}{gf} = \frac{2\alpha g\dot{f}}{f^2}, \tag{3.10}$$

where

$$\alpha = \left(\frac{A_0'}{B_0}\right)_\Sigma. \tag{3.11}$$

Motivated from [50], if we assume $g(t) = f(t)$, Eq. (3.10) reduces to a single ordinary differential equation in the collapse function $f(t)$. This simplification allows direct integration, yielding an explicit solution for $f(t)$, with integration constants determined from the appropriate boundary conditions

$$\dot{f} = 2\alpha f + \beta\sqrt{f}, \tag{3.12}$$

$$t = \frac{1}{\alpha}\ln\left(1 + \frac{2\alpha}{\beta}\sqrt{f}\right). \tag{3.13}$$

Here, β denotes an arbitrary constant arising from the integration of the dynamical equation, and the constant of integration appearing in Eq. (3.13) has been removed through an appropriate redefinition (shift) of the time coordinate t, without loss of generality. The solutions given in (3.12) and (3.13) are identical to the solution presented by [10,12] in the particular case $g(t) = 1$. This establishes the consistency of the present model with earlier results in the appropriate limit.

For a collapsing configuration, the condition $\dot{f}(t) \leq 0$ is required so that the collapse function decreases monotonically with time. From Eq. (3.12), this implies the restriction $\beta \leq -2\alpha$, since $f(t)$ remains positive during the evolution. In order that $\dot{f} \to 0$ as $f \to 1$, corresponding to an initially static limit, we set $\beta = -2\alpha$. With this choice, the solutions (3.1), (3.2), and (3.13) approach the static perfect-fluid configuration asymptotically as $f \to 1$. As time progresses, the system departs gradually from equilibrium and evolves into a non-adiabatic, radiating collapse, thereby modeling the transition from an initially static stellar configuration to a dynamically collapsing and dissipative state.

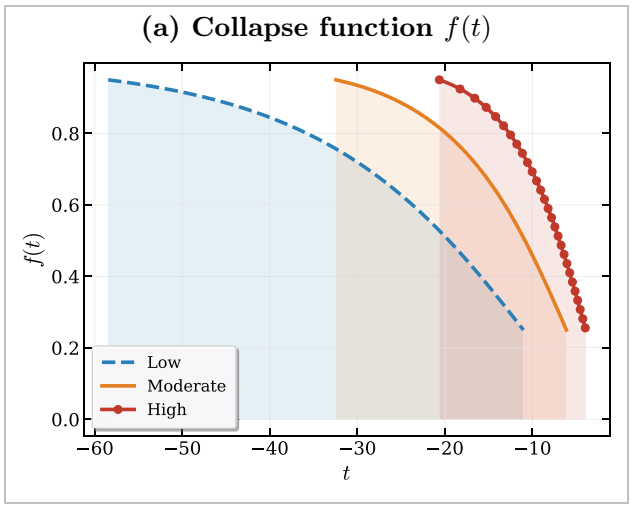

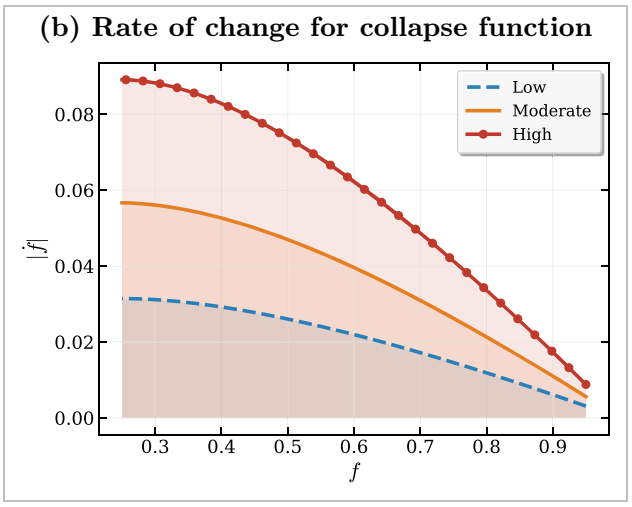

Fig. 1 The temporal evolution of collapse function and modulus of its derivative for $C_1 = 0.25$ (low), $C_1 = 0.50$ (moderate), and $C_1 = 0.90$ (high). All remaining parameters are given in Table 2. The plot **b** is to be read in reverse f going from 1 to 0 and therefore increase in rate of collapse implies increase in collapse rate with higher anisotropy

With the choice $\beta = -2\alpha$, Eqs. (3.12) and (3.13) reduce to simplified forms in which the collapse function and its time derivative depend explicitly on α:

$$\dot{f} = -2\alpha\sqrt{f}\left(1-\sqrt{f}\right), \tag{3.14}$$

$$t = \frac{1}{\alpha}\ln\left(1-\sqrt{f}\right). \tag{3.15}$$

We observe from Fig. 1 that the collapse function $f(t)$ decreases monotonically during the evolution from its initial limiting value toward the final stage. We shall show in the subsequent analysis that the parameter α is related to the anisotropy parameter C_1, see Eq. (6.16).

4 New parametric class of exact solutions

In view of Eqs. (3.4) and (3.5), which provide the explicit forms of the radial and tangential pressures in terms of the metric functions and their derivatives, we analyze the evolution of pressure anisotropy during collapse. Suppose the anisotropy factor is assumed to evolve according to

$$\kappa(p_t - p_r) = \Delta(r,t) = \frac{\delta(r)}{B_0^2(r)\, f^2(t)}, \tag{4.1}$$

where $\delta(r)$ is an arbitrary function of the radial coordinate and $B_0(r)$ and $f(t)$ represent the static and temporal parts of the metric potential, respectively. Substituting this assumed form of $\Delta(r,t)$ into the expressions obtained from Eqs. (3.4) and (3.5), we observe that the explicit time dependence through $f(t)$ cancels out. As a result, the anisotropy condition separates into purely radial and temporal components, and the governing relation reduces to a differential equation involving only the radial coordinate. Consequently, we obtain a time-independent differential equation for the metric potentials. This equation determines the radial structure of the anisotropic stellar model and ensures that the assumed form of anisotropy is consistent with the field equations throughout the collapse:

$$\frac{A_0''}{A_0} + \frac{B_0''}{B_0} - \frac{A_0'}{rA_0} - \frac{B_0'}{rB_0} - \frac{2B_0'^2}{B_0^2} - \frac{2A_0'B_0'}{A_0B_0} - \delta(r) = 0. \tag{4.2}$$

To simplify the highly nonlinear structure of Eq. (4.2), we introduce an ad hoc relation between the static metric potentials of the form $A_0(r) = B_0^n(r)\, A_1(r)$, where n is a constant parameter and $A_1(r)$ is an auxiliary function to be determined. This assumption provides additional flexibility in constructing solutions while preserving the generality of the model.

Substituting this relation into Eq. (4.2) and carrying out the required differentiation, the equation reduces to

$$(n+1)\frac{B_0''}{B_0} + (n^2-3n-2)\frac{B_0'^2}{B_0^2} - (n+1)\frac{B_0'}{rB_0} + \frac{A_1''}{A_1} - \frac{A_1'}{rA_1} + (2n-2)\frac{B_0'}{B_0}\frac{A_1'}{A_1} - \delta(r) = 0. \tag{4.3}$$

This expression clearly separates the contributions arising from the metric potential $B_0(r)$, the auxiliary function $A_1(r)$, and the anisotropy parameter $\delta(r)$. To further simplify the system, we now stipulate the anisotropy parameter in the specific form

$$\delta(r) = (2n-2)\frac{B_0'}{B_0}\frac{A_1'}{A_1}, \tag{4.4}$$

and simultaneously impose the condition

$$\frac{A_1''}{A_1} - \frac{A_1'}{rA_1} = 0. \tag{4.5}$$

The choice of the anisotropy function is guided by the requirement that the anisotropy condition remain compatible with the separable metric ansatz and reduce to a purely radial relation. In particular, the form (4.1) removes the explicit time dependence from the pressure-difference equation, while the further choice (4.4), together with the condition (4.5), decouples the remaining terms in Eq. (4.3). As a result, the system reduces to an integrable differential equation involving only the metric potential $B_0(r)$, thereby leading to a new parametric class of exact anisotropic solutions.

Integration with respect to r gives,

$$A_1(r) = d_2(1 + d_1 r^2), \tag{4.6}$$

where d_1 and d_2 are integration constants.

The assumptions (4.4) and (4.5) reduce the Eq. (4.3) to a simpler, non-linear differential equation involving only $B_0(r)$,

$$(n+1)\frac{B_0''}{B_0} + (n^2 - 3n - 2)\frac{B_0'^2}{B_0^2} - (n+1)\frac{B_0'}{rB_0} = 0. \tag{4.7}$$

The substitution $y = \frac{B_0'}{B_0}$ reduces the above equation to

$$y' + \left(\frac{n^2 - 2n - 1}{n+1}\right) y^2 - \frac{1}{r} y = 0, \tag{4.8}$$

which is a standard Bernoulli equation and may be solved for u by putting $u = 1/y$. Finally we get

$$y(r) = \frac{2r}{\frac{n^2-2n-1}{n+1} r^2 + 2C} \tag{4.9}$$

where C is some constant of integration. Again integrating for B_0 using $y = \frac{B_0'}{B_0}$, we get

$$B_0(r) = C_2 \left(1 + C_1 r^2\right)^{\frac{n+1}{n^2-2n-1}} \tag{4.10}$$

By applying our initial ad hoc relation $A_0(r) = B_0^n(r) A_1(r)$ to combine these independent solutions, we arrive at a new parametric class of exact solutions characterized by the parameter n. The resulting family of solutions represents anisotropic stellar configurations in which the structure of the anisotropy is intrinsically linked to the geometry through the chosen functional relationship between the metric potentials [51]:

$$B_0 = C_2 \left(1 + C_1 r^2\right)^{\frac{1}{l+1}}, \text{ where } \frac{1}{l+1} = \frac{n+1}{n^2 - 2n - 1} \tag{4.11}$$

$$A_0 = D_2 \left(1 + D_1 r^2\right) \left(1 + C_1 r^2\right)^{\frac{n}{l+1}}, \tag{4.12}$$

$$\delta(r) = \frac{(2n-2)}{(l+1)} \frac{4 D_1 C_1 r^2}{(1 + D_1 r^2)(1 + C_1 r^2)}, \tag{4.13}$$

where n, l, C_1, C_2, D_1, and D_2 are constants. Solving $\frac{1}{l+1} = \frac{n+1}{n^2-2n-1}$ for n yields

$$n = \frac{1}{2}\left\{(l+3) \pm \left(l^2 + 10l + 17\right)^{1/2}\right\}. \tag{4.14}$$

From (4.14), n is real if $l^2 + 10l + 17 \geq 0$, or $(l+5)^2 \geq 8$, hence $l \geq -5 + 2\sqrt{2}$ or $l \leq -5 - 2\sqrt{2}$.

5 General structure for collapsing radiating star

In this section, we distinguish between the static variables and the corresponding dynamical variables of the collapsing radiating configuration. The quantities ϵ_0, $(p_r)_0$, and $(p_t)_0$ denote the matter variables of the initial static configuration determined by the metric potentials $A_0(r)$ and $B_0(r)$. The time-dependent variables $\epsilon(r,t)$, $p_r(r,t)$, $p_t(r,t)$, and $q(r,t)$ are obtained from these quantities through the collapse function $f(t)$.

In view of Eqs. (3.3)–(3.6), together with (4.11) and (4.12), the explicit analytical forms of the matter variables characterizing the collapsing radiating star can be obtained. By substituting the corresponding metric functions and auxiliary relations into the Einstein field equations, one derives closed-form expressions for the energy density, radial pressure, tangential pressure, and heat flux:

$$\kappa\epsilon = \frac{\epsilon_0}{f^2} + \frac{12\alpha^2\left(1 - \sqrt{f}\right)^2}{f^3\left[D_2\left(1 + D_1 r^2\right)\left(1 + C_1 r^2\right)^{\frac{n}{l+1}}\right]^2}, \tag{5.1}$$

$$\kappa p_r = \frac{(p_r)_0}{f^2} + \frac{4\alpha^2\left(1 - \sqrt{f}\right)}{f^{5/2}\left[D_2\left(1 + D_1 r^2\right)\left(1 + C_1 r^2\right)^{\frac{n}{l+1}}\right]^2}, \tag{5.2}$$

$$\kappa p_t = \frac{(p_t)_0}{f^2} + \frac{4\alpha^2\left(1 - \sqrt{f}\right)}{f^{5/2}\left[D_2\left(1 + D_1 r^2\right)\left(1 + C_1 r^2\right)^{\frac{n}{l+1}}\right]^2}, \tag{5.3}$$

$$\kappa q = \frac{4r}{(l+1)D_2^2 C_2^2\left(1 + C_1 r^2\right)^{\frac{n+2}{l+1}+1}\left(1 + D_1 r^2\right)^2}\Big[(l+1)D_1\left(1 + C_1 r^2\right) + nC_1\left(1 + D_1 r^2\right)\Big]\frac{2\alpha\left(1 - \sqrt{f}\right)}{f^{7/2}}. \tag{5.4}$$

Using Eqs. (2.8), (3.14), (3.15), (4.11), and (4.12), the expression for the fluid collapse rate is obtained directly by substituting the relevant metric functions and dynamical relations into its kinematical definition. The resulting formula expresses the collapse rate in terms of the time derivative of the collapse function and the associated metric potentials, clearly showing its dependence on the dynamical evolution of the system:

$$\Theta = \frac{-6\alpha\left(1 - \sqrt{f}\right)}{f^{3/2}\left[D_2\left(1 + D_1 r^2\right)\left(1 + C_1 r^2\right)^{\frac{n}{l+1}}\right]}. \tag{5.5}$$

Here, Eqs. (5.1)–(5.4) give the dynamical matter variables of the radiating configuration, while Eq. (5.5) gives the corresponding collapse rate. The quantities ϵ_0, $(p_r)_0$, and $(p_t)_0$ appearing in these expressions are the static variables, whereas α is the boundary parameter entering the temporal evolution through the junction condition. These quantities are given by

$$\epsilon_0 = \frac{4C_1}{(l+1)^2C_2^2\left(1+C_1r^2\right)^{\frac{2}{l+1}+2}}\left[-3(l+1)-(l+2)C_1r^2\right], \tag{5.6}$$

$$(p_r)_0 = \frac{4C_1}{(l+1)^2C_2^2\left(1+C_1r^2\right)^{\frac{2}{l+1}+2}}\Bigg[(l+1)(n+1) + \{(l+1)(n+1)+(2n+1)\}C_1r^2 + \frac{(l+1)D_1\left(1+C_1r^2\right)}{C_1\left(1+D_1r^2\right)}\left\{(l+1)+(l+3)C_1r^2\right\}\Bigg], \tag{5.7}$$

$$(p_t)_0 = \frac{4C_1}{(l+1)^2C_2^2\left(1+C_1r^2\right)^{\frac{2}{l+1}+2}}\Bigg[(l+1)(n+1) + \{(l+1)(n+1)+(2n+1)\}C_1r^2 + \frac{(l+1)D_1\left(1+C_1r^2\right)}{C_1\left(1+D_1r^2\right)} \left\{(l+1)+(l+2n+1)C_1r^2\right\}\Bigg], \tag{5.8}$$

$$\alpha = \frac{2D_2r_\Sigma\left(1+C_1r_\Sigma^2\right)^{\frac{n-l-2}{l+1}}}{C_2(l+1)}\left[nC_1\left(1+D_1r_\Sigma^2\right) + (l+1)D_1\left(1+C_1r_\Sigma^2\right)\right]. \tag{5.9}$$

6 Specific structure for the collapsing radiating star

In this section, we specialize the general model to the case $n = -2$. We first present the static metric variables corresponding to this choice. The dynamical quantities of the radiating model, namely ϵ, p_r, p_t, q, and Θ, are obtained subsequently from the general expressions in Sect. 5.

One can obtain a wide range of physically distinct solutions by assigning different values to the parameter n. Specifically, when $n = 0$, the model describes a configuration with homogeneous energy density accompanied by anisotropic pressure distribution. For $n = 1$, the solution corresponds to homogeneous density with isotropic pressure, indicating equality between the radial and tangential pressures. In the case $n = -1$, the model yields isotropic pressure as well.

However, in order to preserve both inhomogeneity in the energy density and anisotropy in the pressure components, we choose $n = -2$. Substituting this value into Eqs. (4.11)–(4.13) and (5.6)–(5.8), we obtain the static variables for the model as follows:

$$A_0 = D_2\left(1+D_1r^2\right)\left(1+C_1r^2\right)^{2/7}, \tag{6.1}$$

$$B_0 = C_2\left(1+C_1r^2\right)^{-1/7}, \tag{6.2}$$

$$\delta(r) = \frac{24D_1C_1r^2}{7\left(1+D_1r^2\right)\left(1+C_1r^2\right)}, \tag{6.3}$$

$$\epsilon_0 = \frac{4C_1}{49C_2^2\left(1+C_1r^2\right)^{12/7}}\left[21+6C_1r^2\right], \tag{6.4}$$

$$(p_r)_0 = \frac{4C_1}{49C_2^2\left(1+C_1r^2\right)^{12/7}}\left[(7+4C_1r^2) + \frac{7D_1\left(1+C_1r^2\right)\left(7+5C_1r^2\right)}{C_1\left(1+D_1r^2\right)}\right], \tag{6.5}$$

$$(p_t)_0 = \frac{4C_1}{49C_2^2\left(1+C_1r^2\right)^{12/7}}\left[(7+4C_1r^2) + \frac{7D_1\left(1+C_1r^2\right)\left(7+11C_1r^2\right)}{C_1\left(1+D_1r^2\right)}\right]. \tag{6.6}$$

The junction condition $\left((p_r)_0\right)_\Sigma = 0$ in view of $(p_r)_\Sigma = (qB)_\Sigma$, (6.5) gives

$$D_1 = \frac{-C_1\left(7+4C_1r_\Sigma^2\right)}{7\left(1+C_1r_\Sigma^2\right)\left(7+5C_1r_\Sigma^2\right)+C_1r_\Sigma^2\left(7+4C_1r_\Sigma^2\right)}. \tag{6.7}$$

The central values of the static variables are obtained by evaluating ϵ_0, $(p_r)_0$, and $(p_t)_0$ at the center of the configuration. These are given by

$$\epsilon_0 = \frac{12C_1}{7C_2^2}, \tag{6.8}$$

$$(p_r)_0 = \frac{4C_1}{7C_2^2}\left[1+\frac{7D_1}{C_1}\right], \tag{6.9}$$

$$(p_t)_0 = \frac{4C_1}{7C_2^2}\left[1+\frac{7D_1}{C_1}\right]. \tag{6.10}$$

We observe that $\epsilon_0 > 0, (p_r)_0 > 0, (p_t)_0 > 0, \frac{(p_r)_0}{\epsilon_0} < 1$, $\epsilon_0' < 0$, $p_0' < 0$ at the centre are satisfied with suitable choice of constants $C_1 > 0$, $C_2 > 0$, and $-\frac{C_1}{7} < D_1 < 0$ and for the metric $A_0 > 0$, $D_2 > 0$.

Substituting the specialized metric functions (6.1) and (6.2) into the general dynamical expressions (5.1)–(5.5), we obtain

$$\kappa\epsilon = \frac{\epsilon_0}{f^2} + \frac{12\alpha^2\left(1-\sqrt{f}\right)^2}{f^3\left[D_2\left(1+D_1r^2\right)\left(1+C_1r^2\right)^{2/7}\right]^2}, \tag{6.11}$$

Table 2 Parameter values used in the numerical evaluation. The constant D_1 is computed from Eq. (6.7) and α from Eq. (6.16) for each value of C_1

Parameter	Low	Moderate	High
C_1	0.25	0.50	0.90
C_2	1.0	1.0	1.0
D_2	1.0	1.0	1.0
r_Σ	1.0	1.0	1.0
D_1	− 0.0298	− 0.0540	− 0.0849
α	0.0660	0.1189	0.1808
γ (thermal)	0.05	0.05	0.05
Ω	3	3	3

$$\kappa p_r = \frac{(p_r)_0}{f^2} + \frac{4\alpha^2\left(1-\sqrt{f}\right)}{f^{5/2}\left[D_2\left(1+D_1r^2\right)\left(1+C_1r^2\right)^{2/7}\right]^2}, \tag{6.12}$$

$$\kappa p_t = \frac{(p_t)_0}{f^2} + \frac{4\alpha^2\left(1-\sqrt{f}\right)}{f^{5/2}\left[D_2\left(1+D_1r^2\right)\left(1+C_1r^2\right)^{2/7}\right]^2}, \tag{6.13}$$

$$\kappa q = \frac{4r\left[2C_1+D_1\left(7+9C_1r^2\right)\right]}{7D_2^2C_2^2\left(1+C_1r^2\right)\left(1+D_1r^2\right)^2}\,\frac{2\alpha\left(1-\sqrt{f}\right)}{f^{7/2}}, \tag{6.14}$$

$$\Theta = \frac{-6\alpha\left(1-\sqrt{f}\right)}{f^{3/2}\left[D_2\left(1+D_1r^2\right)\left(1+C_1r^2\right)^{2/7}\right]}, \tag{6.15}$$

where by using (5.9) and (6.7) we get

$$\alpha = \frac{2C_1D_2\,r_\Sigma}{7C_2\left(1+C_1r_\Sigma^2\right)^{4/7}}. \tag{6.16}$$

The physical parameters such as anisotropy parameter $\delta(r)$, density $\kappa\epsilon(r,t)$, mass function at boundary $M_\Sigma(f)$, boundary red-shift $z_\Sigma(f)$, and pressures are plotted in Fig. 2. The physical parameters ϵ, p_r, p_t remain finite and positive throughout the interior of the configuration. Within the radial domain $0 \le r \le r_\Sigma$ these quantities exhibit a smooth and monotonic decrease as the radial coordinate increases from the center toward the boundary surface. Moreover, their first derivatives with respect to the radial coordinate are negative everywhere in this interval, indicating that the energy density and both radial and tangential pressures continuously diminish outward without any irregular behavior or divergence.

By substituting the explicit forms of the relevant physical and metric functions given in Eqs. (3.1), (3.2), (3.3), (3.14), (6.1), (6.2), and (6.16) into Eq. (2.16), the energy expression can be rewritten in a more explicit and simplified form as

$$M(v) = \left[\frac{8}{49}\,\frac{C_1^2C_2\,r_\Sigma^5\left(1-\sqrt{f}\right)^2}{\left(1+C_1r_\Sigma^2\right)^{13/7}\left(1+D_1r_\Sigma^2\right)^2} + m_0 f\right]_\Sigma, \tag{6.17}$$

where

$$m_0 = \frac{2}{49}\,\frac{C_1C_2\,r_\Sigma^3\left(7+6C_1r_\Sigma^2\right)}{\left(1+C_1r_\Sigma^2\right)^{15/7}}. \tag{6.18}$$

Using Eqs. (2.17)–(3.2), (3.14), (6.1), (6.2), and (6.16), the expressions for the surface luminosity, the boundary redshift at Σ, and the luminosity measured by a distant observer at rest at infinity are obtained in explicit form:

$$L_\Sigma = \frac{8}{49}\left[\frac{C_1r_\Sigma^2}{(1+C_1r_\Sigma^2)(1+D_1r_\Sigma^2)}\right]^2\frac{\left(1-\sqrt{f}\right)}{\sqrt{f}}, \tag{6.19}$$

$$L_\infty = \frac{8}{49}\left[\frac{C_1r_\Sigma^2}{(1+C_1r_\Sigma^2)(1+D_1r_\Sigma^2)}\right]^2\frac{\left(1-\sqrt{f}\right)}{\sqrt{f}}\,\frac{1}{(1+z_\Sigma)^2}, \tag{6.20}$$

with

$$z_\Sigma = \frac{\left[\frac{\left(1+D_1r_\Sigma^2\right)\left(7+5C_1r_\Sigma^2\right)\sqrt{f}+4C_1r_\Sigma^2\left(1-\sqrt{f}\right)}{7\left(1+C_1r_\Sigma^2\right)\left(1+D_1r_\Sigma^2\right)}\right]_\Sigma}{\left(1-\frac{2M}{rB_0f}\right)_\Sigma} - 1. \tag{6.21}$$

These quantities z_Σ and L_Σ are plotted in Figs. 2d and 3a. Equations (6.20) and (6.21) indicate that the luminosity observed at L_∞ approaches zero as $f(t) \to 1$ and as the boundary condition $(rB_0f)_\Sigma \to 2M_\Sigma$ is satisfied, signifying the approach to horizon formation. This behavior reflects the complete trapping of radiation as the collapsing configuration reaches the Schwarzschild radius. Further, by making use of Eqs. (3.15), (6.17), and (6.18), the time of black hole formation corresponding to the instant when the collapse reaches the horizon, that is, $(rB_0f)_\Sigma \to 2M_\Sigma(v)$, can be determined. The resulting expression provides the collapse time in terms of the model parameters and boundary quantities, thereby specifying the epoch at which the event horizon forms:

$$\sqrt{f}_{BH} = \frac{4C_1r_\Sigma^2}{4C_1r_\Sigma^2+\left(1+D_1r_\Sigma^2\right)\left(7+5C_1r_\Sigma^2\right)}, \tag{6.22}$$

and

$$t_{BH} = \frac{1}{\alpha}\ln\left[\frac{\left(1+D_1r_\Sigma^2\right)\left(7+5C_1r_\Sigma^2\right)}{4C_1r_\Sigma^2+\left(1+D_1r_\Sigma^2\right)\left(7+5C_1r_\Sigma^2\right)}\right]. \tag{6.23}$$

Horizon formation time t_{BH} is plotted in Fig. 3b.

7 Energy conditions and temperature evolution

To ensure the physical viability of the obtained solutions, we examine the standard energy conditions, namely the Null Energy Condition (NEC), Weak Energy Condition (WEC),

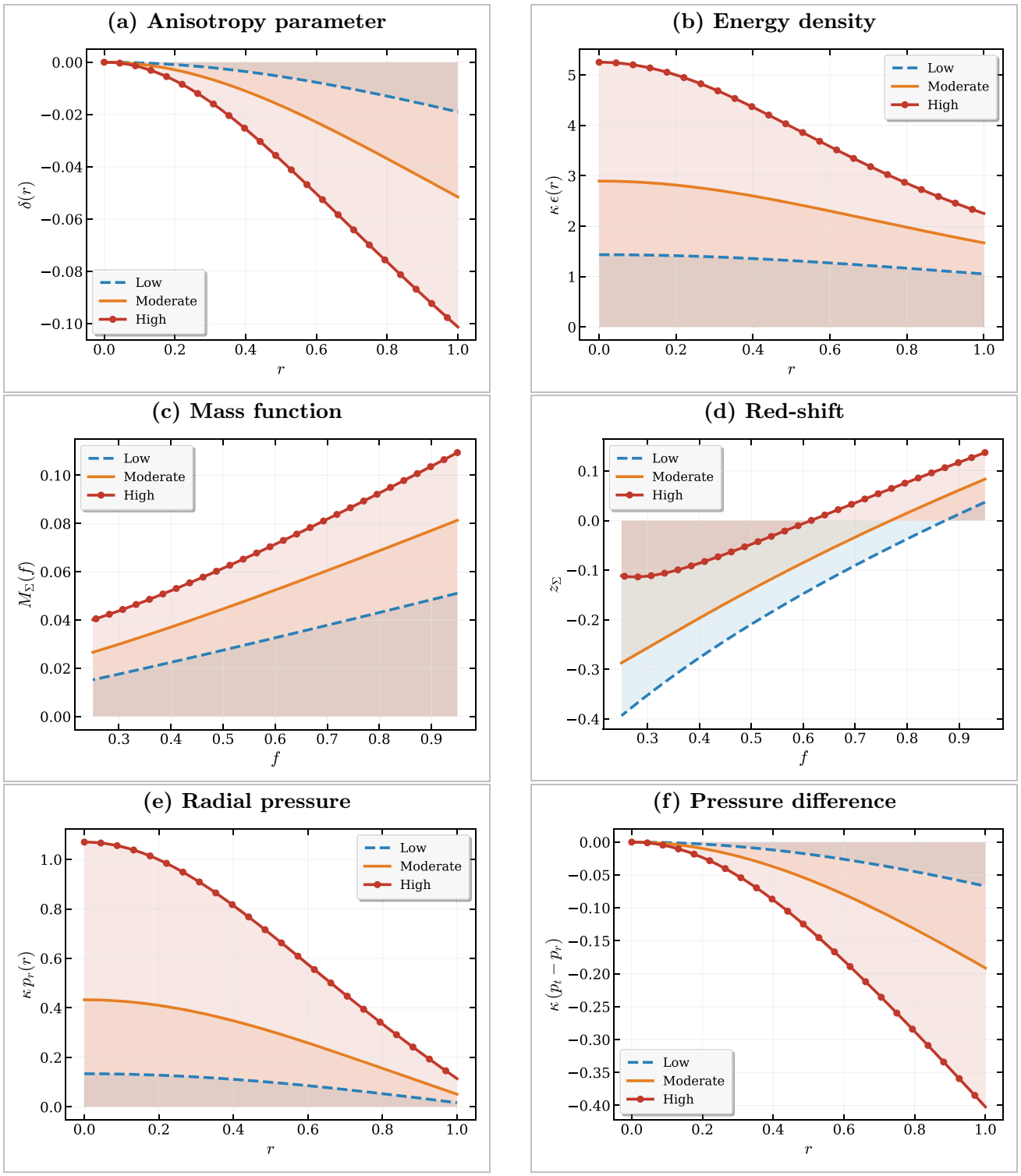

Fig. 2 Variations of anisotropy, density, mass function, red-shift, radial pressure and the anisotropy indicator pressure difference for $C_1 = 0.25$ (low), $C_1 = 0.50$ (moderate), and $C_1 = 0.90$ (high). All remaining parameters are given in Table 2

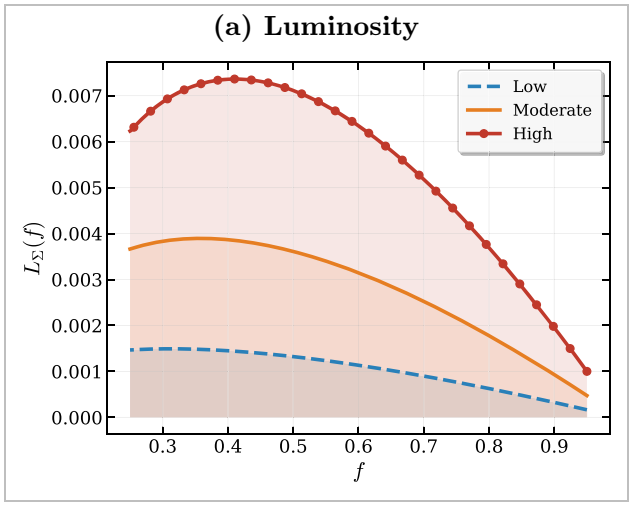

Fig. 3 **a** The variation of luminosity for $C_1 = 0.25$ (low), $C_1 = 0.50$ (moderate), and $C_1 = 0.90$ (high). **b** Time of horizon formation vs anisotropy. As anisotropy increases, the time to horizon formation decreases, as evidenced by the narrowing of the shaded (blue) region in **b**. All remaining parameters are given in Table 2

Strong Energy Condition (SEC), and Dominant Energy Condition (DEC). For an anisotropic fluid distribution, these conditions require:

1. NEC: $\epsilon + p_r \geq 0 \quad \text{and} \quad \epsilon + p_t \geq 0$,
2. WEC: $\epsilon \geq 0, \quad \epsilon + p_r \geq 0, \quad \text{and} \quad \epsilon + p_t \geq 0$,
3. SEC: $\epsilon + p_r + 2p_t \geq 0$,
4. DEC: $\epsilon - |p_r| \geq 0 \quad \text{and} \quad \epsilon - |p_t| \geq 0$.

From Fig. 4, it is evident that all four combinations – $\epsilon + p_r, \epsilon, \epsilon + p_r + 2p_t$, and $\epsilon - |p_r|$ – remain strictly positive throughout the stellar interior for all three parametric configurations (Low, Moderate, and High). Each quantity attains its maximum value at the centre and decreases monotonically toward the boundary, yet remains well above zero at all radii.

Within the framework of extended irreversible thermodynamics, heat transport in the collapsing matter is described by a causal Maxwell–Cattaneo type relation. In the truncated Israel–Stewart theory, this transport equation incorporates a finite relaxation time and governs the evolution of temperature and heat flux in a manner consistent with relativistic causality, as developed by Werner Israel and subsequent authors [52–54]:

$$\tau\left(g^{\mu\nu} + w^\mu w^\nu\right) w^\alpha q_{\nu;\alpha} + q^\mu = -\mathbb{K}\left(g^{\mu\nu} + w^\mu w^\nu\right)\left[T_{,\nu} + T\dot{w}_\nu\right], \tag{7.1}$$

where $\mathbb{K}\ (\geq 0)$ denotes the thermal conductivity and $\tau\ (\geq 0)$ represents the relaxation time associated with the heat flux. To obtain a simplified estimate of the temperature evolution, one may neglect relaxation effects by setting $\tau = 0$ in Eq. (7.1). Under this assumption, the transport equation reduces to the non-causal form, yielding a simpler relation governing the temperature distribution:

$$q = -\mathbb{K}\frac{1}{B_0^2 f^2}\left(T' + T\frac{A_0'}{A_0}\right) = -\frac{2A_0'\dot{f}}{A_0^2 B_0^2 f^4}. \tag{7.2}$$

The magnitude of heat flux is plotted in Fig. 5a.

Assuming the thermal conductivity to be of the form $\mathbb{K} = \gamma T^\Omega \geq 0$, where γ and Ω are positive constants, Eq. (7.2) can be integrated to obtain the corresponding expression for the temperature distribution:

$$T^{\Omega+1} = \frac{T_0(t)}{A_0^{\Omega+1}} - \frac{4(\Omega+1)}{\gamma\Omega}\frac{\alpha}{A_0}\frac{\left(1-\sqrt{f}\right)}{f^{3/2}}, \tag{7.3}$$

where $T_0(t)$ is an arbitrary function of t.

The effective surface temperature as measured by a distant external observer can be determined from the corresponding relation given by Karl Schwarzschild [55]:

$$T_\Sigma^4 = \left\{\frac{1}{\pi\delta(rB_0 f)^2}\right\}_\Sigma, \tag{7.4}$$

$$L_\infty = \frac{8}{49}\frac{C_1^2 r_\Sigma^2}{\pi\delta C_2^2\left(1+C_1 r_\Sigma^2\right)^{12/7}\left(1+D_1 r_\Sigma^2\right)^2}\frac{\left(1-\sqrt{f}\right)}{f^{5/2}}\frac{1}{\left(1+z_\Sigma\right)^2}, \tag{7.5}$$

where for photons the constant δ is given by

$$\delta = \frac{\pi^2 k^4}{15\hbar^3}, \tag{7.6}$$

where k and $\hbar$ denote respectively the Boltzmann and Planck constants.

By selecting $\Omega = 3$, which corresponds to radiation interacting with matter under the diffusive approximation as dis-

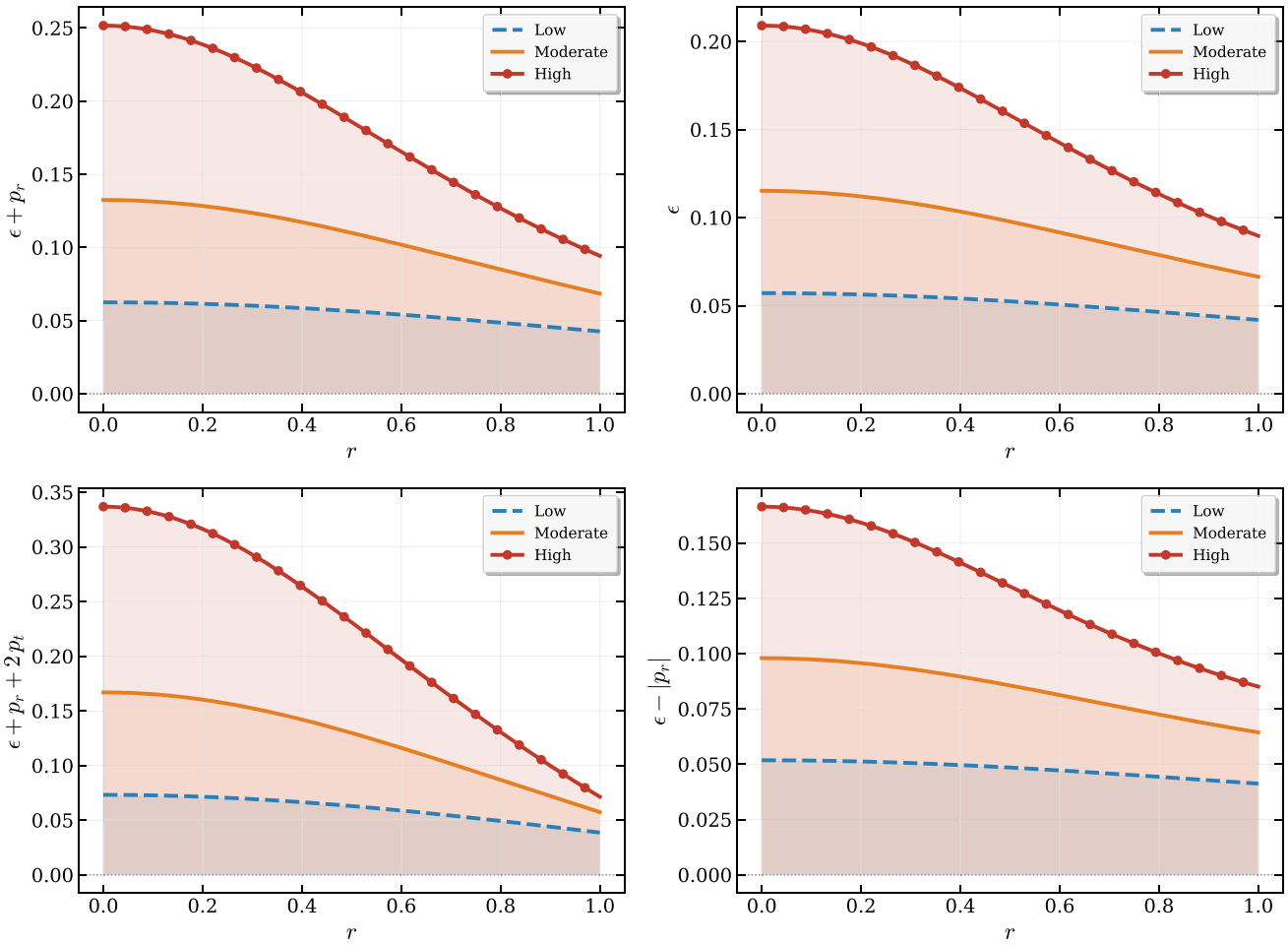

Fig. 4 The radial evolution of radial and tangential pressures for $C_1 = 0.25$ (low), $C_1 = 0.50$ (moderate), and $C_1 = 0.90$ (high). All remaining parameters are given in Table 2

cussed by Charles Misner and David Sharp [56], the model is specialized to the radiative transport regime. The arbitrary function $T_0(t)$ can then be determined by utilizing Eqs. (7.3) and (7.4), yielding the corresponding expression:

$$T_0(t) = \left\{ \frac{16\alpha}{3k} \left[D_2\left(1 + D_1 r^2\right)\left(1 + C_1 r^2\right)^{2/7} \right]^3 \frac{\left(1 - \sqrt{f}\right)}{f^{3/2}} \right\}_{\Sigma} + \left\{ \frac{2\alpha^2}{\left[D_2\left(1 + D_1 r^2\right)\left(1 + C_1 r^2\right)^{2/7} \right]^2 \pi \delta r^2} \frac{\left(1 - \sqrt{f}\right)}{f^{5/2}} \right\}_{\Sigma} \frac{1}{(1 + z_{\Sigma})^2}. \tag{7.7}$$

Temperature inside the star is given by:

$$T^4 = \frac{T_0(t)}{\left[D_2\left(1 + D_1 r^2\right)\left(1 + C_1 r^2\right)^{2/7} \right]^4} - \frac{16}{3\gamma \left[D_2\left(1 + D_1 r^2\right)\left(1 + C_1 r^2\right)^{2/7} \right]} \frac{\left(1 - \sqrt{f}\right)}{f^{3/2}}, \tag{7.8}$$

which is plotted in Fig. 5b.

8 Conclusion

We investigated shear-free, spherically symmetric, anisotropic gravitational collapse with radiative heat flow, matched smoothly to a Vaidya exterior. Focusing on the inhomogeneous anisotropic case $n = -2$, we derived closed-form expressions for the matter variables, kinematical scalars, Misner–Sharp mass, surface luminosities, boundary redshift, and the black-hole formation time.

Numerical results for three representative values of the anisotropy parameter δ through C_1 show that anisotropy effectively speeds up collapse. Larger C_1 increases the energy density and both pressure components throughout the interior, strengthens $\Delta = p_t - p_r$ away from the centre, and produces a faster contraction. Consistently, the horizon formation time t_{BH} decreases as anisotropy grows. The boundary redshift z_{Σ} is enhanced at each epoch. The interior temperature also rises with C_1, consistent with stronger heat flux and accelerated collapse. For the adopted parameter range, the solution satisfies the null, weak, strong, and dominant

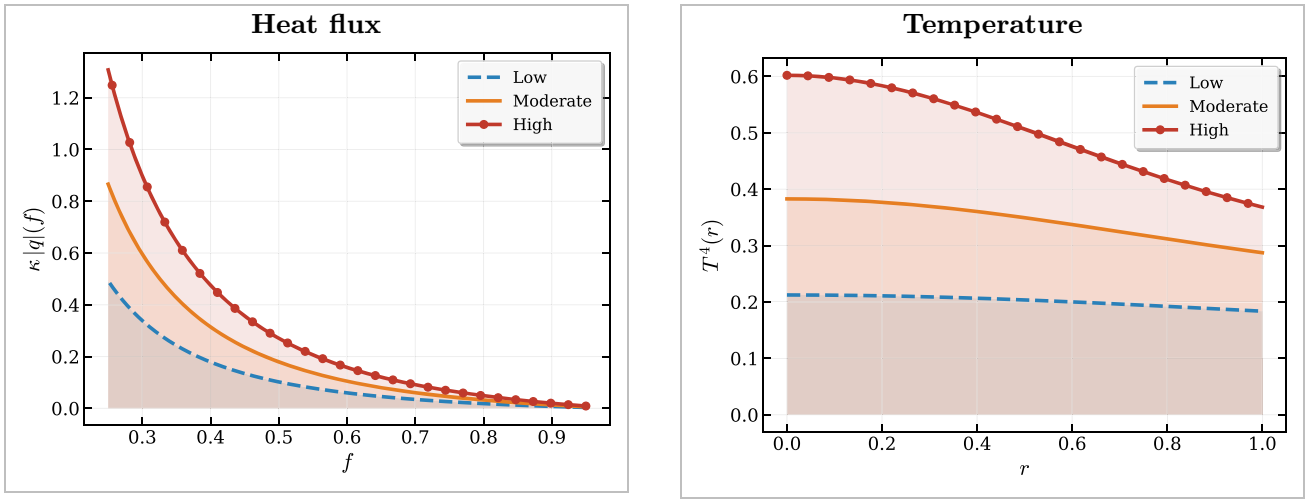

Fig. 5 Heat flux and temperature for $C_1 = 0.25$ (low), $C_1 = 0.50$ (moderate), and $C_1 = 0.90$ (high). All remaining parameters are given in Table 2

energy conditions throughout the interior. The future works in this direction could include charge, viscosity, and rotation.

Acknowledgements OP Yadav acknowledges the support from the Anusandhan National Research Foundation (ANRF), Government of India, Department of Higher Education, India, under Project no. ANRF/ARGM/2025/002254/MTR. We also thank the anonymous referees for their valuable comments and suggestions.

Data Availability Statement This manuscript has no associated data. [Author's' comment: Data sharing is not applicable to this article as no datasets were generated or analysed during the current study.]

Code Availability Statement Code/software will be made available on reasonable request. [Author's comment: The code/software generated during and/or analysed during the current study is available from the corresponding author on reasonable request.]

Funded by SCOAP[3].

References

1. A. Abac, I. Abouelfettouh, F. Acernese, K. Ackley, C. Adamcewicz, S. Adhicary, D. Adhikari, N. Adhikari, R. Adhikari, V. Adkins et al., Gw231123: a binary black hole merger with total mass 190–265 $m_\odot$. Astrophys. J. Lett. **993**(1), L25 (2025)
2. A. Einstein, Die Feldgleichungen der Gravitation, Sitzungsberichte der Königlich Preussischen Akademie der Wissenschaften, pp. 844–847 (1915)
3. K. Schwarzschild, Über das Gravitationsfeld eines Massenpunktes nach der Einsteinschen Theorie, Sitzungsberichte der Königlich Preussischen Akademie der Wissenschaften, pp. 189–196 (1916)
4. S. Chandrasekhar, The maximum mass of ideal white dwarfs. Astrophys. J. **74**, 81–82 (1931)
5. J.R. Oppenheimer, H. Snyder, On continued gravitational contraction. Phys. Rev. **56**, 455–459 (1939)
6. P.C. Vaidya, The gravitational field of a radiating star. Proc. Indian Acad. Sci. A **33**, 264–276 (1951)
7. R.W. Lindquist, R.A. Schwartz, C.W. Misner, Vaidya's radiating Schwarzschild metric. Phys. Rev. **137**, B1364–B1368 (1965)
8. N.O. Santos, Non-adiabatic radiating collapse. Mon. Not. R. Astron. Soc. **216**, 403–410 (1985)
9. E. Glass, Shear-free gravitational collapse. J. Math. Phys. **20**(7), 1508–1513 (1979)
10. A.K.G. de Oliveira, N.O. Santos, C.A. Kolassis, Collapse of a radiating star. Mon. Not. R. Astron. Soc. **216**, 1001–1011 (1985)
11. A.K.G. de Oliveira, N.O. Santos, Non-adiabatic gravitational collapse. Astrophys. J. **312**, 640–645 (1987)
12. W.B. Bonnor, A.K.G. de Oliveira, N.O. Santos, Radiating spherical collapse. Phys. Rep. **181**, 269–326 (1989)
13. S.D. Maharaj, M. Govender, Radiating collapse with vanishing Weyl stresses. Int. J. Mod. Phys. D **14**, 667–676 (2005)
14. B.V. Ivanov, Self-gravitating spheres of anisotropic fluid in geodesic flow. Int. J. Mod. Phys. D **20**, 319–334 (2011)
15. A. Banerjee, S. Chatterjee, N. Dadhich, Spherical collapse with heat flow and without horizon. Mod. Phys. Lett. A **17**, 2335–2339 (2002)
16. L. Herrera, N.O. Santos, Dynamics of dissipative gravitational collapse. Phys. Rev. D **70**, 084004 (2004)
17. B. Tewari, K. Charan, Radiating star, shear-free gravitational collapse without horizon. Astrophys. Space Sci. **351**(2), 613–617 (2014)
18. R. Chan, Collapse of a radiating star with shear. Mon. Not. R. Astron. Soc. **288**(3), 589–595 (1997)
19. S.D. Maharaj, M. Govender, Collapse of a charged radiating star with shear. Pramana J. Phys. **54**, 715–727 (2000)
20. G. Abebe, S. Maharaj, K. Govinder, Generalized Euclidean stars with equation of state. Gen. Relativ. Gravit. **46**(5), 1733 (2014)

21. G. Govender, B.P. Brassel, S.D. Maharaj, The effect of a two-fluid atmosphere on relativistic stars. Eur. Phys. J. C **75**(7), 324 (2015)
22. S.D. Maharaj, B.P. Brassel, Radiating stars with composite matter distributions. Eur. Phys. J. C **81**(4), 366 (2021)
23. S.D. Maharaj, B.P. Brassel, Radiating composite stars with electromagnetic fields. Eur. Phys. J. C **81**(9), 783 (2021)
24. R.L. Bowers, E.P.T. Liang, Anisotropic spheres in general relativity. Astrophys. J. **188**, 657–665 (1974)
25. B.C. Paul, P.K. Chattopadhyay, S. Karmakar, Relativistic anisotropic star and its maximum mass in higher dimensions. Astrophys. Space Sci. **356**(2), 327–337 (2015)
26. S. Maurya, Y. Gupta, S. Ray, D. Deb, Generalised model for anisotropic compact stars. Eur. Phys. J. C **76**(12), 693 (2016)
27. G. Raposo, P. Pani, M. Bezares, C. Palenzuela, V. Cardoso, Anisotropic stars as ultracompact objects in general relativity. Phys. Rev. D **99**(10), 104072 (2019)
28. A. Saha, K. Goswami, P. Chattopadhyay, Anisotropic star in Vaidya–Tikekar model admitting MIT bag model equation of state in pseudo-spheroidal geometry. Astrophys. Space Sci. **366**(10), 98 (2021)
29. B. Das, S. Dey, S. Das, B.C. Paul, Anisotropic compact objects with Finch–Skea geometry in EGB gravity. Eur. Phys. J. C **82**(6), 519 (2022)
30. A. Saha, K. Goswamiy, B. Dasz, P. Chattopadhyayx, Maximum mass of anisotropic charged strange quark stars in a higher dimensional approach (D$\geq$ 4). Chin. Phys. C **47**(1), 015107 (2023)
31. S. Thirukkanesh, S. Maharaj, Charged anisotropic matter with a linear equation of state. Class. Quantum Gravity **25**(23), 235001 (2008)
32. L. Herrera, N.O. Santos, Local anisotropy in self-gravitating systems. Phys. Rep. **286**, 53–130 (1997)
33. M. Cosenza, L. Herrera, M. Esculpi, L. Witten, Some models of anisotropic spheres in general relativity. J. Math. Phys. **22**, 118–125 (1981)
34. S.S. Bayin, Anisotropic fluid spheres in general relativity. Phys. Rev. D **26**, 1262–1274 (1982)
35. L. Herrera, A.D. Prisco, J. Ospino, Some analytical models of radiating collapsing spheres. Phys. Rev. D **74**, 044001 (2006)
36. G. Estevez-Delgado, J. Estevez-Delgado, On the effect of anisotropy on stellar models. Eur. Phys. J. C **78**(8), 673 (2018)
37. L. Gabbanelli, Á. Rincón, C. Rubio, Gravitational decoupled anisotropies in compact stars. Eur. Phys. J. C **78**(5), 370 (2018)
38. L.L. Lopes, H. Das, Role of local anisotropy in hybrid stars. Eur. Phys. J. C **84**(10), 1049 (2024)
39. K.P. Reddy, M. Govender, S.D. Maharaj, Impact of anisotropic stresses during dissipative gravitational collapse. Gen. Relativ. Gravit. **47**, 35 (2015)
40. S. Das, R. Sharma, B.C. Paul, R. Deb, Dissipative gravitational collapse of an (an) isotropic star. Astrophys. Space Sci. **361**(3), 99 (2016)
41. S. Maharaj, G. Govender, M. Govender, Temperature evolution during dissipative collapse. Pramana **77**(3), 469–476 (2011)
42. B.V. Ivanov, A different approach to anisotropic spherical collapse with shear and heat radiation. Int. J. Mod. Phys. D **25**, 1650049 (2016)
43. B.V. Ivanov, All solutions for geodesic anisotropic spherical collapse with shear and heat radiation. Astrophys. Space Sci. **361**, 18 (2016)
44. A. Mahomed, S. Maharaj, R. Narain, A generating function and new exact solutions for geodesic matter. Afr. Mat. **32**(1), 17–29 (2021)
45. K. Charan, O.P. Yadav, B. Tewari, Charged anisotropic spherical collapse with heat flow. Eur. Phys. J. C **81**(1), 60 (2021)
46. Y. P. Singh, Badruddin, Study of short-term periodicities in the occurrence of forbush decreases: wavelet analysis. Astrophys. Space Sci. **369**(7), 66 (2024)
47. S.D. Maharaj, K.S. Govinder, Dynamics of the temporal evolution in radiating stars. Gen. Relativ. Gravit. **57**(1), 11 (2025)
48. S.K. Maurya, A. Ashraf, A. Ali, M. Govender, F. Javed, P. Channuie, Modeling anisotropic compact objects in the vanishing complexity regime through gravitational decoupling. Eur. Phys. J. C **85**(10), 1–14 (2025)
49. M. Singh, Y.P. Singh, A multi-parametric comparative study of solar cycles 23, 24, and 25 using solar and interplanetary disturbance indices. Astrophys. Space Sci. **371**(3), 35 (2026)
50. B.C. Tewari, Collapsing shear-free radiating fluid spheres. Gen. Relativ. Gravit. **45**, 1547–1558 (2013)
51. B. Tewari, K. Charan, Horizon free eternally collapsing anisotropic radiating star. Astrophys. Space Sci. **357**(2), 107 (2015)
52. W. Israel, J.M. Stewart, Transient relativistic thermodynamics and kinetic theory. Ann. Phys. (N.Y.) **118**, 341–372 (1979)
53. R. Maartens, Dissipative cosmology. Class. Quantum Gravity **12**, 1455–1465 (1995)
54. J. Martínez, Transport processes in the gravitational collapse of an anisotropic fluid. Phys. Rev. D **53**, 6921–6940 (1996)
55. M. Schwarzschild, *Structure and Evolution of the Stars* (Princeton University Press, Princeto, 1958)
56. C.W. Misner, D.H. Sharp, Relativistic equations for adiabatic, spherically symmetric gravitational collapse. Phys. Rev. **136**, B571–B576 (1964)